On the natural causes of global warming

Research article

Abstract

Aims/ Objectives: To illustrate natural origins of global warming
Methodology: It is demonstrated that temperature anomalies in 1900 – 2009 are inextricably linked to the speed of the magnetic North Pole, used as a proxy for the Earth's magnetic field; and UFO sightings, used as a proxy for energy transfer from the near-terrestrial space to the Earth's atmosphere. Also explained is why 2010 – 2016 was a very unusual period and how it affected global temperature and the environment.
Conclusion: Current global warming is an entirely natural process driven by forces of Nature.

Keywords: Global warming, Earth's magnetic field, undetermined areal phenomena.

1 Introduction

We demonstrate a striking similarity between instrumentally measured temperature, the speed of the magnetic North Pole as a proxy for the Earth's magnetic field, and UFO sightings as a proxy for energy transfer between near-Earth space and the Earth's atmosphere. While many a pundit stridently clamor that UFOs are indicative of extraterrestrial aliens, we show that UFOs are but a facet in a large-scale natural phenomenon of solar-terrestrial origin.

The similarity between global temperature and several other distinct and seemingly unrelated natural phenomena points towards the natural origin of global warming, which goes contrary to the current 97% consensus that global warming is caused by the greenhouse effect resulting from increased levels of CO_2. Since the average temperature on Earth is around 287K, the current temperature anomalies of 1K represent $\approx \frac{1}{287} < 0.4\%$; that is the relative contribution to global temperature discussed in the paper.

2 Section 2. Materials and Methods

We use and compare data and graphs produced by reputable research agencies such as but not limited to NOAA, NASA, USGS.

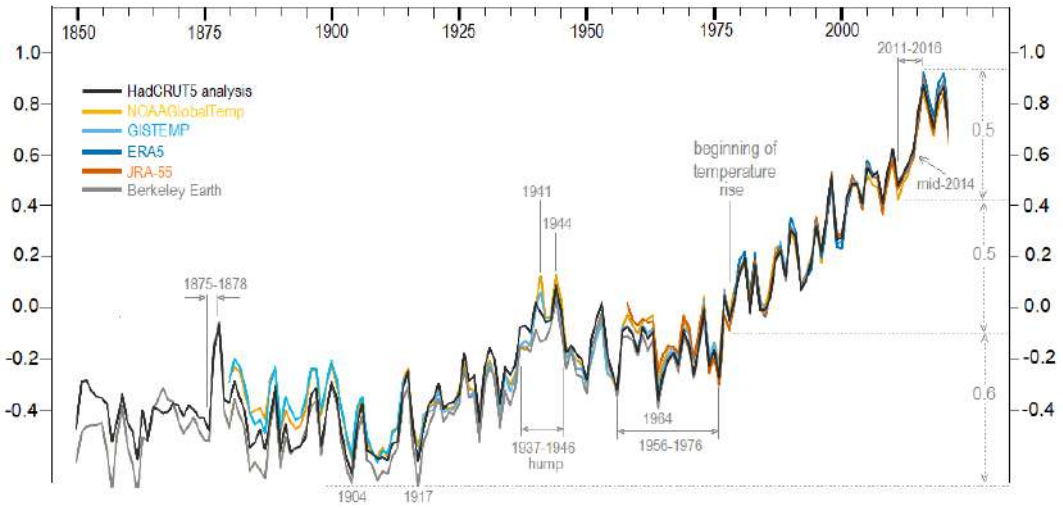

Figure 1: Annual global temperature anomalies in $^{\circ}C$ in 1900 – 2020 by six agencies, [1]. The largest known uninterrupted increase in global temperature occurred in 2011 – 2016.

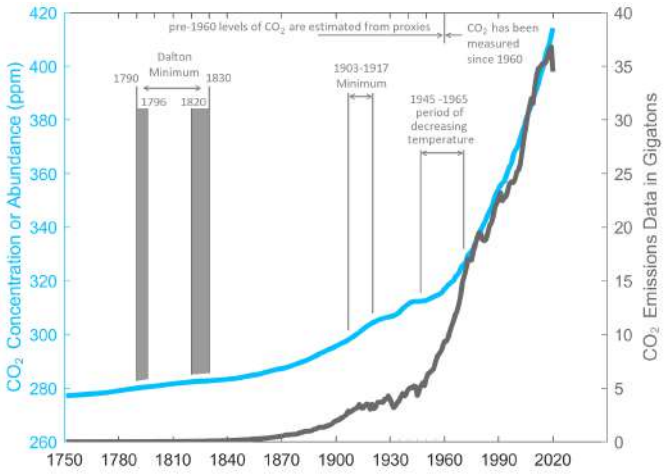

Figure 2: CO_2 concentration and emission. The original graph was produced and kindly emailed to the author of this paper by Dr. Howard Diamond, Climate Science Program Manager, NOAA. Comments were added by the author of this paper. The graph of CO_2 concentration bears no resemblance to and shows no correlation with the graphs in Figure 1, other than that CO_2 concentration and the graphs in Figures 1 increased in 1980 – 2020. Nor is the 1903 – 1917 temperature minimum reflected in the CO_2 graph in any way; as a matter of fact, the rate of increase of the CO_2 graph accelerated during the 1903 – 1917 temperature minimum. Even more bemusing is that the 1945 – 1965 period of decreasing temperature in Figure 1 seems to have coexisted with the rising levels of CO_2 shown above. The definition of the Dalton Minimum varies between 1790 – 1830 and 1796 – 1820, both options are shown; yet, whichever time window is chosen, the graph of CO_2 does not give even the tiniest hint of a temperature minimum.

3 Section 3. Results and Discussion

3.1 Review of the 1590 – 1900 period.

As a reference point for global temperature, we use Figure 1 exhibiting measurements by six reputable agencies. Figure 2 shows CO_2 concentration and emission, it bears no resemblance to and shows no correlation with Figure 1, other than that both CO_2 concentration and temperature in Figure 1 increased in 1980 – 2020. Before any discussion about post-1900 temperature increase, consider the climate patterns before 1900. Figure 3 shows that in the pre-1900 age global temperature determined from proxies shadowed the movement of the magnetic North Pole: 1) the Maunder and Dalton Minima coincided with the portions of the magnetic North Pole's path with low speed and low curvature; 2) the two warm periods more-or-less coincided with the portions of the magnetic North Pole's path with either high speed or large curvature. Figure 6 confirms the same relationship between the movement of the magnetic North Pole in 1659 – 1900 and the longest known instrumentally-measured temperature record going back all the way to 1659 — each significant increase in the magnetic North Pole's speed or its path's curvature led to a temperature increased. Figure 4 shows that the regions of the magnetic North Pole's high speed and large curvature were accompanied by high sunspot numbers, while the regions of low speed and small curvature were accompanied by low sunspot numbers. The magnetic North Pole's path shows three U-turns around 1632, 1730, and 1859; while the last two were concurrent with the 1730/10/22 Boston solar flare and the 1859/9/1-2 Carrington solar flare, Figure 5 shows that the 1632 U-turn was accompanied by a drastic increase in recorded auroras indicative of a drastic increase in solar flares.

3.2 The 1900 – 2009 period

Since the path of the magnetic North Pole in 1900 – 2009 was rather flat, the previous section suggests that global temperature should shadow the magnetic North Pole's speed. Figure 7 indeed demonstrates a remarkable similarity in the behavior of the magnetic North Pole's speed and temperature.

Only in one instance does temperature seem to fail to shadow the magnetic North Pole's speed. In pane I of Figure 7, the 1935 maximum in the speed of the magnetic North Pole appears to produce temperatures considerably higher than the larger 1950 maximum. Since the speed of the magnetic North Pole is but a simple facet of the Earth's magnetic field that does reflect all aspects of the latter, we may expect the Earth's magnetic field to reveal disturbance not reflected in the speed of the magnetic North Pole. Indeed, Figure 8 reveals a considerable agitation in the Earth's magnetic field around 1938 – 1952, accompanied by a power tussle described in Figure 9. These co-occurred with 1) the 1938 – 1946 increase in earthquake activity with 13 magnitude $\geqslant 8.0$ earthquakes or 1.44 earthquakes per year, for comparison, 1900 – 1999 saw 70 such earthquakes or 0.7 earthquakes per year, [10]; 2) an unusual increase in the number of unrecognized aerial phenomena, often referred to as foo fighters, unsuccessfully investigated by the Robertson Panel, Projects Sign, Grudge, Blue Book; and 3) 28 unusually powerful auroras on 1936/6/10, 1936/6/19, 1937/2/28, 1937/4/28, 1937/8/3, 1938/1/25 Fatima geomagnetic storm, 1940/3/25, 1940/4/3, 1941/1/18, 1941/7/6, 1941/9/18, 1942/6/27, 1943/9/4, 1944/10/15, 1944/12/17, 1946/2/3, 1946/3/24, 1946/4/8, 1946/7/26, 1947/3/8, 1947/7/19, 1947/8/27, 1948/3/16, 1949/1/27, 1950/2/21, 1950/8/20, 1951/7/2, 1951/9/23, [11]. A large number of powerful auroras suggests a considerable increase in solar activity; indeed, the solar activity must have been affected by a rare configuration of the Solar System illustrated in Figure 10. The resulting increase in the solar activity must have been responsible for the auroras and, at least partially, contributed to the agitation of Figure 8 and additional temperature in 1938 – 1945 in pane I. Yet, it is not clear whether the configuration of

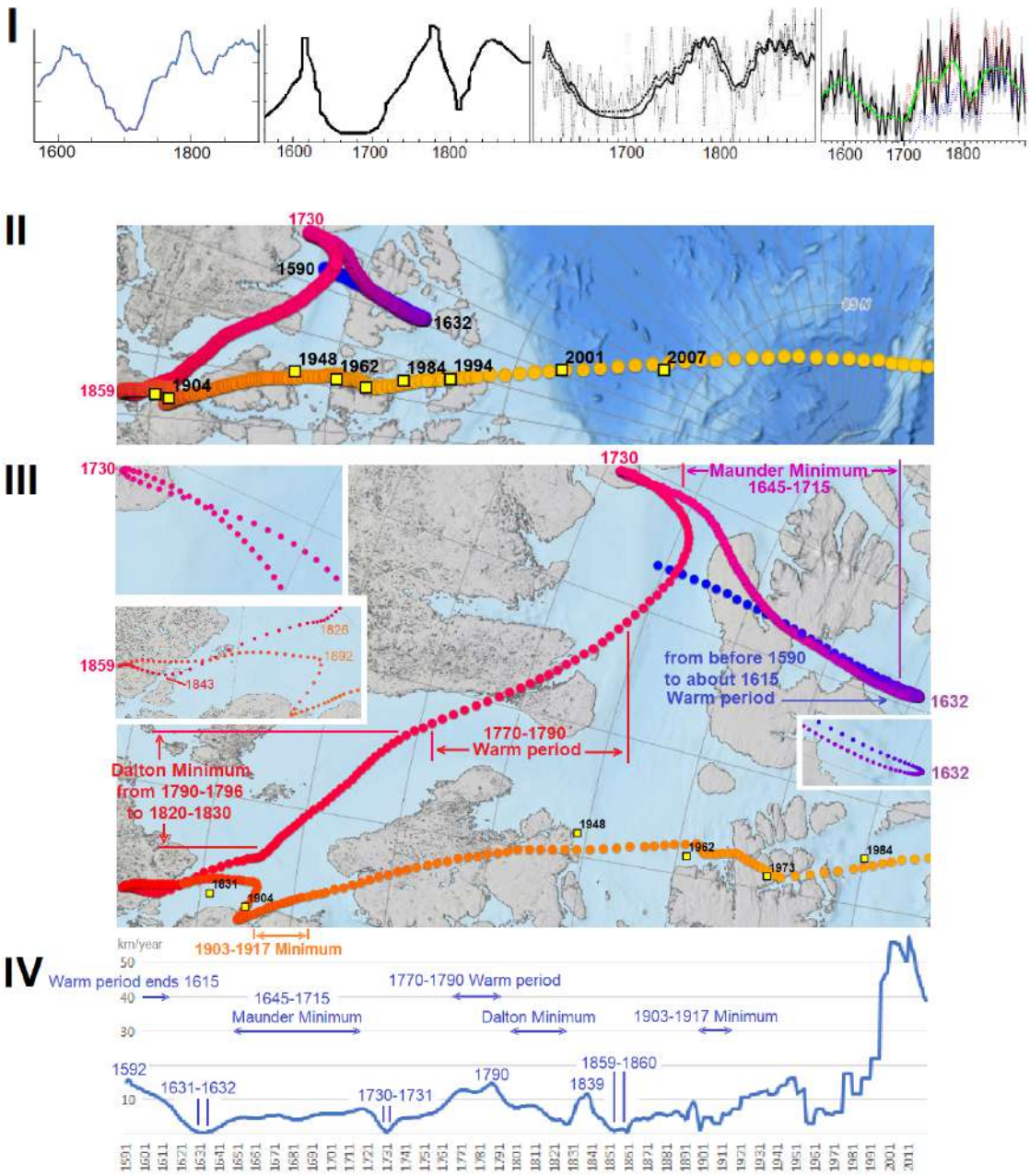

Figure 3: Graph I shows solar activity recovered from different proxies up to 1900, [2]. Graph II shows modeled path of the magnetic North Pole in 1590 – 2022 with yellow squares indicating the actually measured locations, [3]; graph III zooms in on the 1590 – 1980 portion; graph IV shows the speed of the magnetic North Pole constructed from NOAA's data, [4]. In the pre-1900 age, the Maunder and Dalton Minima coincided with the portions of the magnetic North Pole's path with low speed and low curvature, while the two warm periods more-or-less coincided with the portions of the math with either high speed or large curvature.

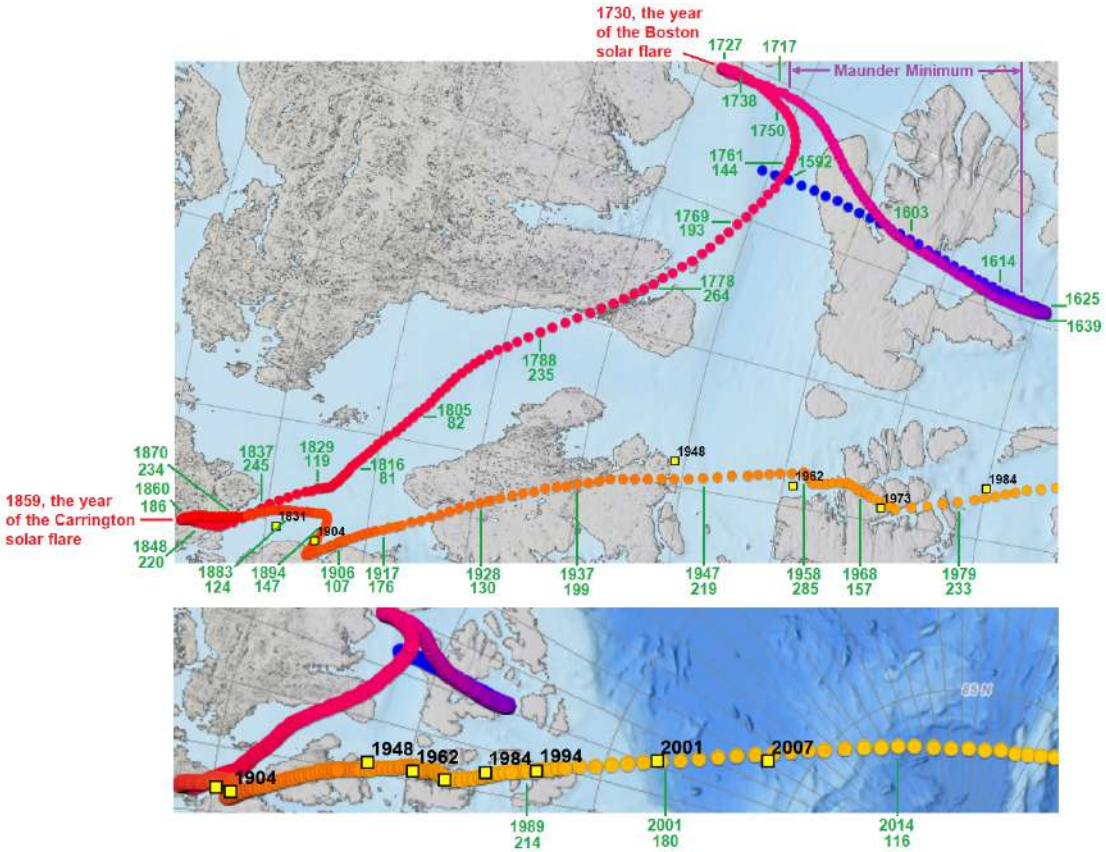

Figure 4: Solar maxima in 1590 – 2021, for 1760 – 2021 sunspot numbers are also shown. There are currently several definitions of sunspot numbers; depending on the definition used, the values of sunspot numbers may vary, the years of solar maxima may also slightly vary. It is easily seen that high sunspot numbers correspond to either increased speed of the magnetic North Pole or increased curvature of its path. Similarly, the low sunspot numbers correspond to the regions of low speed of the magnetic North Pole and small curvature. In 5 out of 6 solar maxima in 1935 – 1991, the sunspot number was $\geqslant 199$; for comparison, that occurred in 5 out of 15 solar maxima in 1760 – 1935. The magnetic North Pole's path shows three U-turns around 1632, 1730, and 1859; the last two were concurrent with the 1730/10/22 Boston solar flare and the 1859/9/1-2 Carrington solar flare, Figure 5 shows that the 1632 U-turn was accompanied by a drastic increase in recorded auroras indicative of a drastic increase in solar flares.

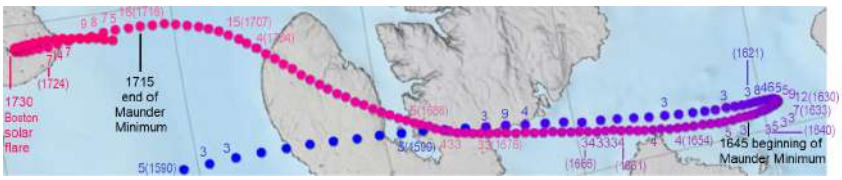

Figure 5: Auroras observed during the Maunder Minimum, [6], shown on the magnetic North Pole's modeled path. The numbers of auroras for each year are shown only for years with $\geqslant 3$ auroras. It shows a drastic increase in auroras contemporaneous with the 1632 U-turn in the path of the magnetic North Pole.

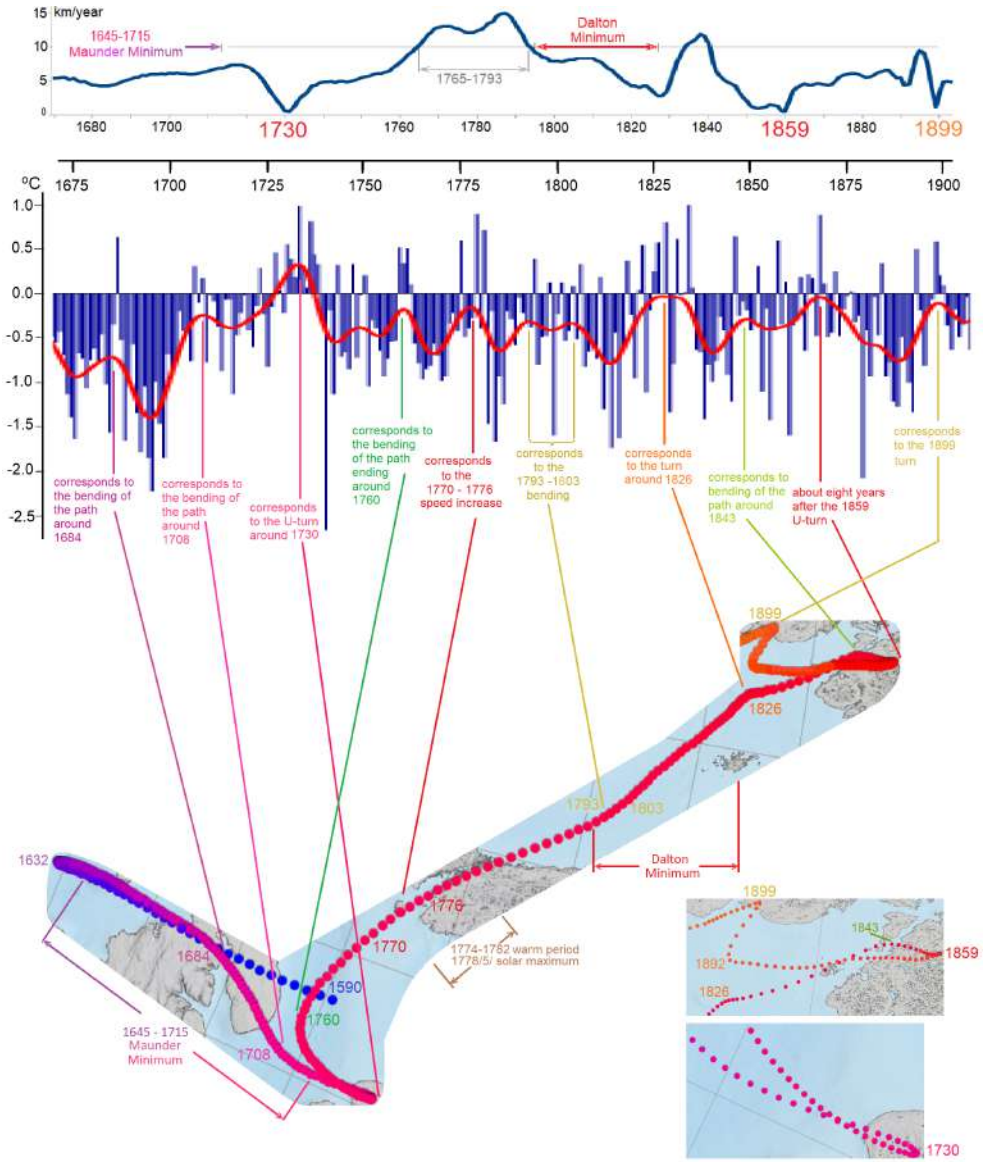

Figure 6: The top graph shows the speed of the magnetic North Pole. The middle graph shows the mean Central England temperature annual anomalies in 1659 – 2010 in blue, their average in red, [5]. The bottom graph shows the 1590 – 1920 portion of the magnetic North Pole's path from Figure 3, two insets zoom in on the crowded portions of the graph. Pre-1900 speed of the magnetic North Pole was insignificant; temperature depended more on the path's curvature than the speed. The maxima of the red curve are matched with the turns of the path giving rise to them; although the matching is not perfect, it is sufficient to indicate the existence of a correlation between temperature and the movement of the magnetic North Pole. Colors are solely for visualization.

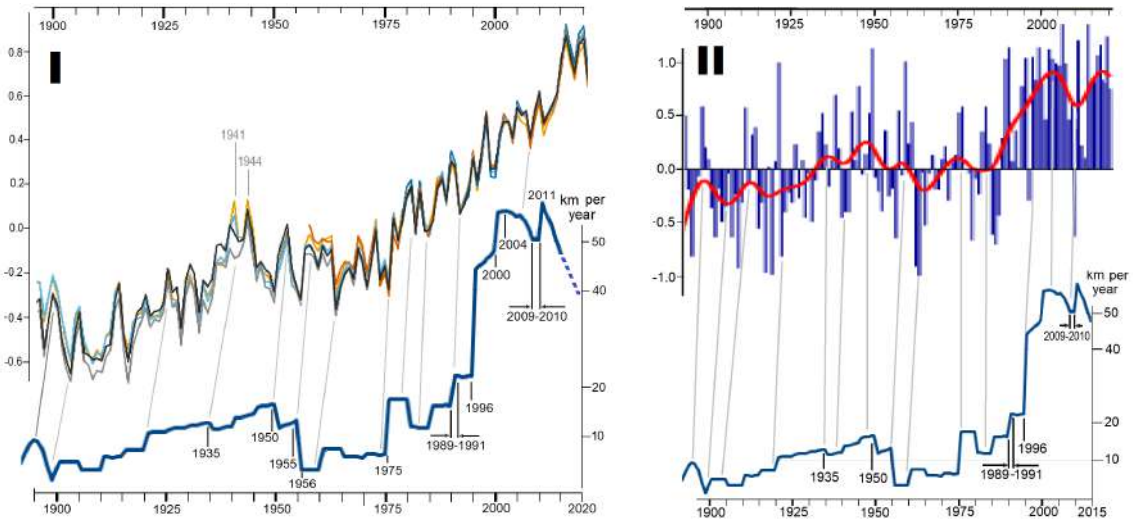

Figure 7: The top graph in pane I shows the 1900 – 2020 portion of Figure 1, the bottom graph shows the speed of the magnetic North Pole constructed from NOAA's data, [4]; the 1900 – 2010 portions of the two graphs exhibit unequivocal similarity, the gray lines indicate which points on the two graphs correspond to each other. The top graph in pane II shows the mean Central England temperature annual anomalies in 1900 – 2010 in blue and its average in red, numerical data is from Met Office, [5], the bottom graph is the speed of the magnetic North Pole; the gray lines indicate which points on the two graphs correspond to each other. The Met's temperature graph is very similar to the temperature record in Uppsala and Stockholm in Figure 1.1e in [7]. The speed of the magnetic North Pole rose above 20 km/year in 1991, at the end of the 1989/3/ – 1991/6/ bombardment by solar flares, of which twelve were $\geqslant X9.3$; it was the heaviest bombardment since the record-keeping began.

Figure 10 co-occurred with geomagnetic events of Figures 8, 9 merely by chance, or there is a deep relationship between them.

The sudden increase in the magnetic North Pole's speed was accompanied by a burst of nine magnitude $\geqslant 7.9$ earthquakes on 1994/6/9, 1994/10/4, 1995/7/30, 1995/10/9, 1995/12/3, 1996/1/1, 1996/2/17, 1996/6/10, 1996/6/17, [10], and two VEI$\geqslant 5$ eruptions on 1991/6/15, 1991/8/8; and preceded by a slew of powerful solar flares: 1989/3/10 X15.0, 1989/8/16 X20.0, 1989/9/29 X9.8, 1989/10/19 X13.0, 1990/5/24 X9.3, 1991/1/25 X10.0, 1991/6/1 X12.0, 1991/6/4 X12.0, 1991/6/6 X12.0, 1991/6/9 X10.0, 1991/6/11 X12.0, 1991/6/15 X12.0, 1992/11/2 X9.0, [29]. It is hard to attribute to a mere coincidence the concomitance of rather unusual events: 1) the 1989 – 1992 solar flare cannonade, 2) the 1994 – 1996 burst in seismic activity, 3) the 1996 acceleration of the magnetic North Pole, 4) the drastic increase in annual temperature in Pane II of Figure 7; they are most likely closely related.

3.3 The 2010 – 2016 period and beyond.

As Figure 7 shows, global temperature and the magnetic North Pole's speed move more-or-less in tandem in 1900 – 2010; around 2011 their behavior diverges with magnetic North Pole's speed going down while the global temperature speeding up. A closer look at the 2010 – 2016 period reveals its very peculiar nature.

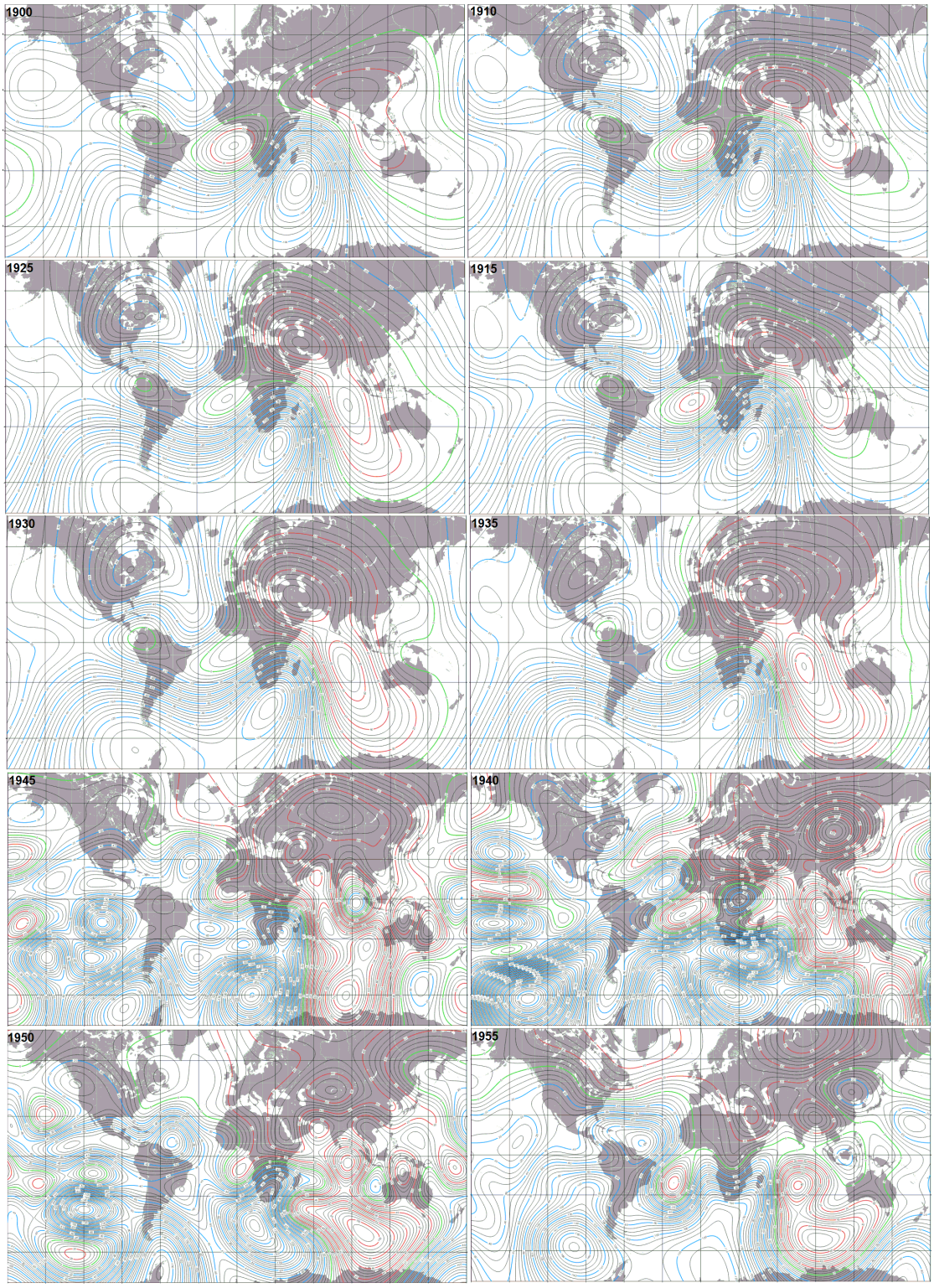
1900
1910
1925
1915
1930
1935
1945
1940
1950
1955

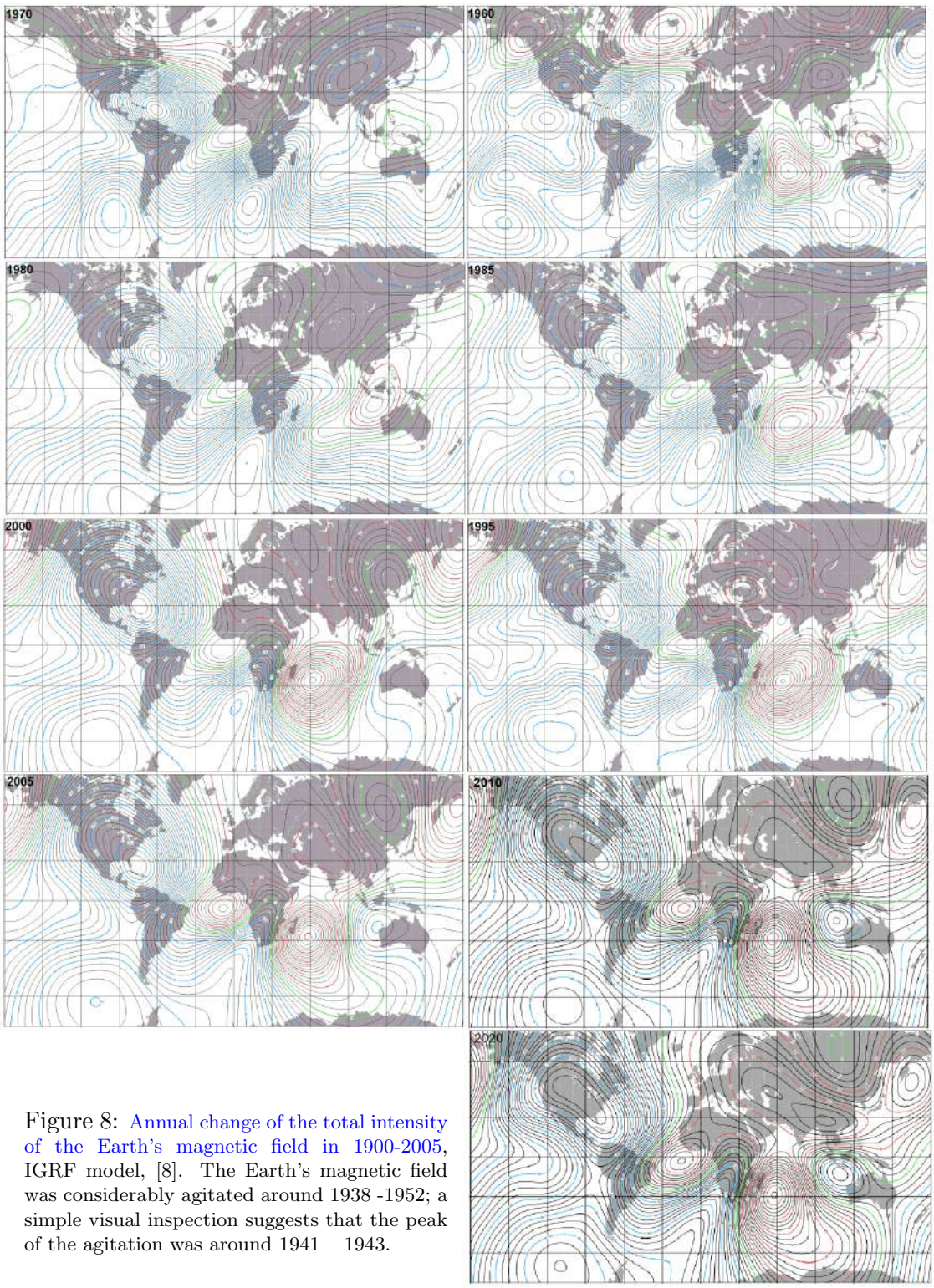

Figure 8: Annual change of the total intensity of the Earth's magnetic field in 1900-2005, IGRF model, [8]. The Earth's magnetic field was considerably agitated around 1938 -1952; a simple visual inspection suggests that the peak of the agitation was around 1941 – 1943.

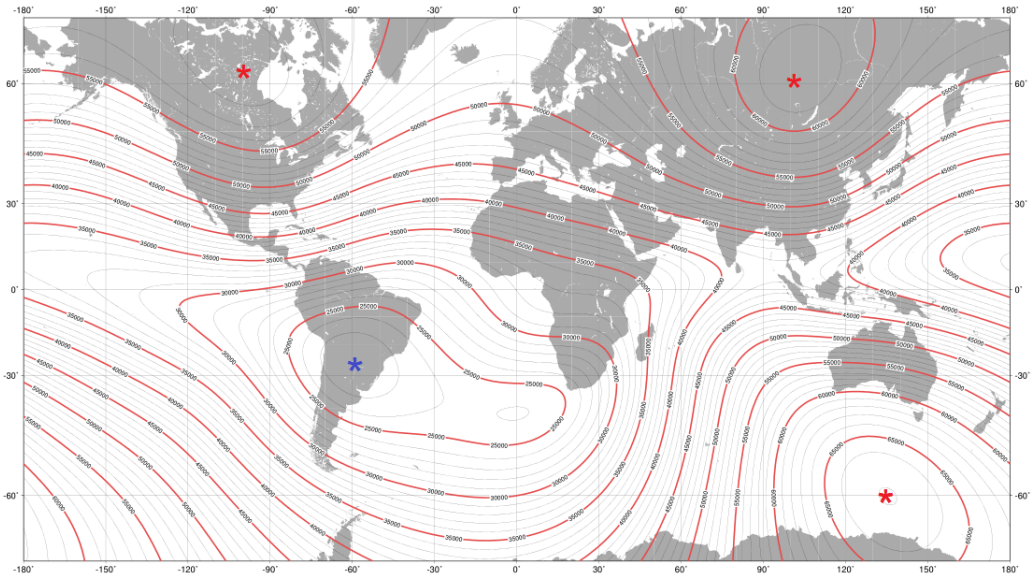

Figure 9: Total intensity of the Earth's magnetic field on 2020/1/1, [8]. The absolute minimum 22 231.9 nT at $26.1^{\circ}S, 59.2^{\circ}W$ is marked by a blue asterisk. The three global maxima are marked by red asterisks: 1) North-Eastern maximum 61 746.1 nT at $61.4^{\circ}N, 102.4^{\circ}E$, merely ≈59 km from the epicenter of the Tunguska explosion at $60.917^{\circ}N, 101.95^{\circ}E$; 2) North-Western maximum 58 632.3 nT at $62.4^{\circ}N, 99.0^{\circ}W$, merely 56 km away from Angikuni Lake at $62.2^{\circ}N, 99.983333^{\circ}W$. 3) Southern maximum 66 991.6 nT at $60.0^{\circ}S, 135.4^{\circ}E$. NOAA's model shows that the relative contribution of the North-Western maximum was larger than that of the North-Eastern maximum before 1948/11/27, while it was smaller after 1948/11/27, [8]. In reality, the tussle for superiority between the two maxima must have lasted for years with the baton changing hands more than once.

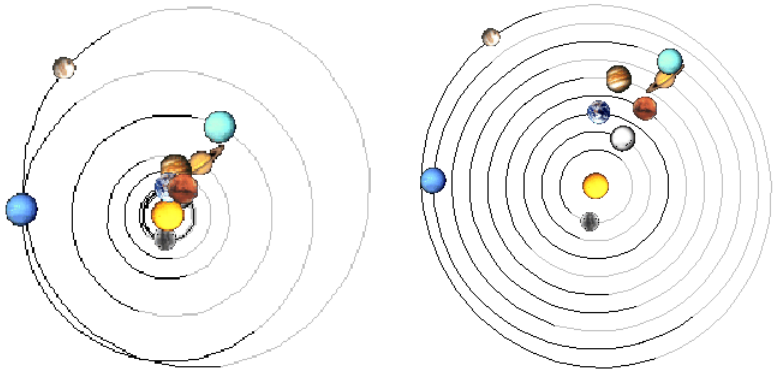

Figure 10: Solar system on 1941/12/18. On the left, orbits are shown in real configuration; on the right, orbits are shown as equidistant circles, [9]. With 1941/12/8 Jupiter opposition, 1941/11/17 Saturn opposition, 1941/11/21 Uranus opposition, 1941/11/10 Mars opposition, and 1942/2/2 Venus conjunction with Sun, 96.1% of the planetary mass of the Solar system almost lined up along a single line; of that Jupiter makes 71.2%, Saturn 21.3%, Uranus 3.3%, Earth 0.2%, and Venus 0.2%. The planets began to align as early as September 1941, the early stages of the alignments were marked by the 1941/9/18-19 geomagnetic storm.

On 2010/1/30, 2011/3/19, 2012/5/6, 2013/6/23, 2014/8/10, 2015/9/28, and 2016/11/14, Full Moon and perigee came within, correspondingly, 165, 59, 2, 23, 27, 65, and 150 minutes of each other synchronizing the increases in tidal pull due to Full Moon and perigee, [12]. Never in the known history have Full Moon and perigee been merely 2 minutes apart as on 2012/5/6; nor have they been $\leqslant$65 minutes apart for 5 years in a row or $\leqslant$165 minutes apart for seven years in a row. The increases in tidal force due to the synchronization of Full Moon and perigee were further amplified by the 2010/1/29, 2012/5/7, 2013/6/20 lunar nodes, and 2015/9/27 eclipse. We shall refer to a pair of a Full Moon and a perigee that come within 11 hours of each other as *Full Moon-perigee*, *New Moon-perigee* is defined similarly. Full Moon-perigees recur on average every 412 - 413 days, and so do New Moon-perigees. On 2010/9/6, 2011/10/26, 2012/12/12, 2014/1/1, 2015/2/19, 2016/4/7 New Moon and perigee came within 9 hours of each other, which by itself is nothing to write home about, but the increase in tidal force was amplified by the 2010/9/4, 2011/10/29, 2012/12/11, 2015/2/21, 2016/4/5 lunar nodes, 2013/1/2, 2014/1/4 perihelia, 2010/9/21, 2011/10/29, 2012/12/3, 2014/1/5, 2015/2/6 Jupiter oppositions, 2010/9/21 Uranus opposition, 2014/1/11 Venus-Sun conjunction, [13].

Although the increase in tidal force was rather small, it nevertheless brought the tidal force close to an all-time high, and must have contributed to unusual terrestrial events: 1) an uninterrupted temperature rise in Figure 1; 2) a never-before-seen alignment of magnitude $\geqslant$ 7.9 earthquakes with Full Moon-perigees shown in Table 1; 3) one of the only two known cases of three magnitude $\geqslant$ 8.5 earthquakes striking three years in a row on 2010/2/27, 2011/3/11, 2012/4/11, accompanied by the 2011/6/30-4 VEI=5 eruption of Puyehue, only once before three powerful earthquakes struck three years in a row on 1963/10/13, 1964/3/28, 1965/2/4, accompanied by the 1963/3/18 VEI=5 eruption of Agung, [10, 14]; 4) the only observed space hurricane detected on 2014/8/20, [16]. The synchronization of Full Moon and perigee may have also contributed to the only known appearance of the third Van Allen Belt on 2012/9/2, followed by waxing and waning of the Belts, obliteration of the outer and middle Belts, and final recovery of the known Belts' structure, [15].

The mid-2014 – early-2015 was marked by never-before-seen undulations in cosmic ray intensity shown in Figure 11 and the mid-2014 jump in the rate of temperature increase in Figure 1. Cosmic rays are known to exhibit 27-day variability attributed to the solar synodic period; but never has the 27-day variability been as clear and well-pronounced as in 2014/6/20 – 2015/2/13. Figure 11 points to the Moon as a significant contributor to the undulations; since the only known source of energetic particles that could be influenced by the Moon is the Van Allen Belts, we must conclude that the undulations were produced by secondary particles created not only by cosmic rays but also by energetic particles from the Van Allen Belts. The tidal force produced by the synchronization of Full Moon and perigee must have "shaken" the Van Allen Belts similarly to magnetopause shadowing, when a solar emission, such as a gust of solar wind or a solar flare, temporarily changes the shape of the Van Allen Belts interfering with the particles' typical drift around magnetic lines and forcing particles in all directions; the only difference is that the tidal force replaces solar emissions and is applied periodically. A similar effect is produced by changes in the Earth's magnetic field, when the changing shape of the magnetic lines interferes with particles' movement leading to the same results as magnetopause shadowing.

While the energy distribution of cosmic rays peaks around 300 MeV with some particles' energy exceeding 10^{20} eV, the energy of protons in the inner Van Allen Belt is typically under 50 MeV, although, according to [19], some may reach $>$ 1 GeV. Are there enough high-energy protons in the Van Allen Belts to affect the cosmic ray monitors? Recent work suggests that electrons may be accelerated to ultra-relativistic energies, [21, 22] with [23] stating outright that energetic electron precipitation from Earth's outer radiation belt contributes to heating the upper atmosphere. We may speculate that from mid-2014 to early 2015, sufficiently many protons in the Van Allen Belts were also accelerated to cosmic ray energies contributing to the undulations. The 2012 – 2015 period produced rather unusual events such as the aforementioned space hurricane detected on 2014/8/20, [16], and the third Van Allen Belt born on 2012/9/2, neither one has been completely

Full Moon-perigees in 2010/1/1 – 2016/12/31	days between	Magnitude ⩾ 7.9 earthquakes in 2010/1/1 – 2016/12/31		
2016/11/14	33	2016/12/17	M=7.9	Papua New Guinea
2015/9/28	12	2015/9/16	M=8.3	Alaska
2014/8/10	48	2014/6/23	M=7.9	Alaska
none		2014/4/1	M=8.2	Chile
2013/6/23	30	2013/5/24	M=8.3	Russia
none		2013/2/6	M=8.0	Solomon Islands
2012/5/6	25	2012/4/11	M=8.2	aftershock
2012/5/6	25	2012/4/11	M=8.6	Indonesia
2011/3/19	8	2011/3/11	M=7.9	aftershock
2011/3/19	8	2011/3/11	M=9.1	Japan
2010/1/30	28	2010/2/27	M=8.8	Chile

Table 1: Alignment of magnitude ⩾ 7.9 earthquakes, [10], with Full Moon-perigees, [12]. Full Moon-perigees recur approximately every 412 - 413 days. In 2010/1/1 – 2017/1/1, ≈91% of M⩾ 7.9 earthquakes struck within 48 days of a Full Moon-perigee. If earthquakes struck randomly, only $\approx \frac{96}{412} \times 11 \leqslant 3$ earthquakes would be expected to strike within 48 days of a Full Moon-perigee; not all 9. The 2014/4/1 earthquake was not within 48 days of a Full Moon-perigee; however, it coincided with the 2014/3/30 – 2014/4/1 New Moon and lunar node and followed a rather unusual coalescence of the 2014/1/1 New Moon-perigee, 2014/1/4 perihelion, 2014/1/5 Jupiter opposition, 2014/1/11 Venus-Sun conjunction, and 2013/12/29 Mercury-Sun conjunction, all resulting in increased tidal force.

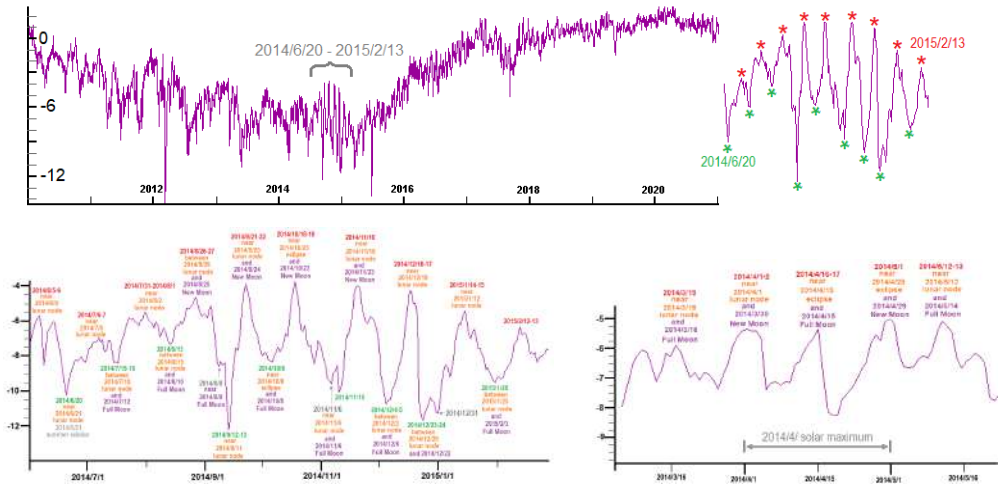

Figure 11: Cosmic rays variations, daily resolution, [17]. It shows rather unusual undulations in 2014/6/20 – 2015/2/13 with the maxima/minima marked correspondingly by red/green. Maxima/minima are close to lunar nodes, maxima are close to New Moon, minima are close to Full Moon, [12]. Although 27-day variability in cosmic rays is well-known, it has never been so strongly exhibited; nor is it well-understood for as [18] points out "existing theoretical models are not able to adequately reproduce characteristics of 27-day variations in the particle flux". The undulations were preceded by the 2014/3/15 – 2014/5/15 14-day recurrence of maxima shown in the bottom right pane, it has no analog in particle flux.

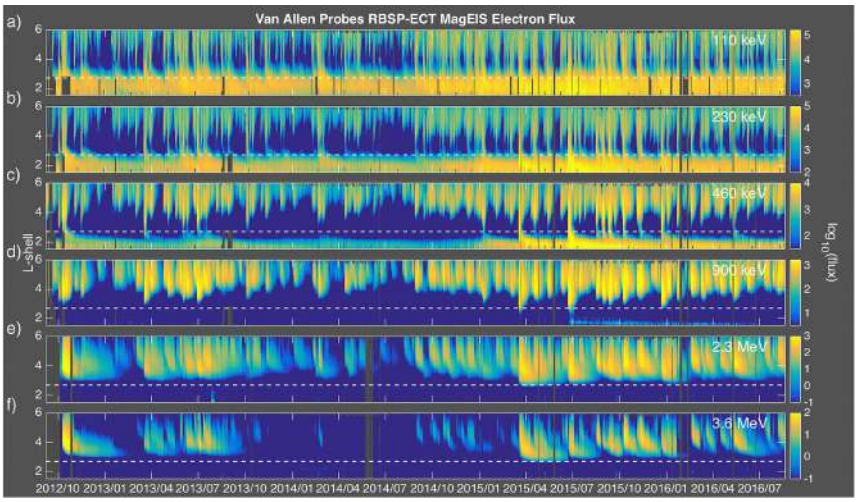

Figure 12: Electron differential fluxes in the inner Van Allen Belt from the MagEIS instruments on the Van Allen Probes spacecraft, [19]. Flux here is in units of $\#/(cm^2 ssr KeV)$. Data from both RBSP A and B are shown in color (log10(flux)) binned in time and L shell during the period from launch in September 2012 through February 2016. From top to bottom, each plot shows results from a different energy channel, as labeled in the top right of each plot. The graph shows flux drop for low L around 2013/10/ – 2015/3/.

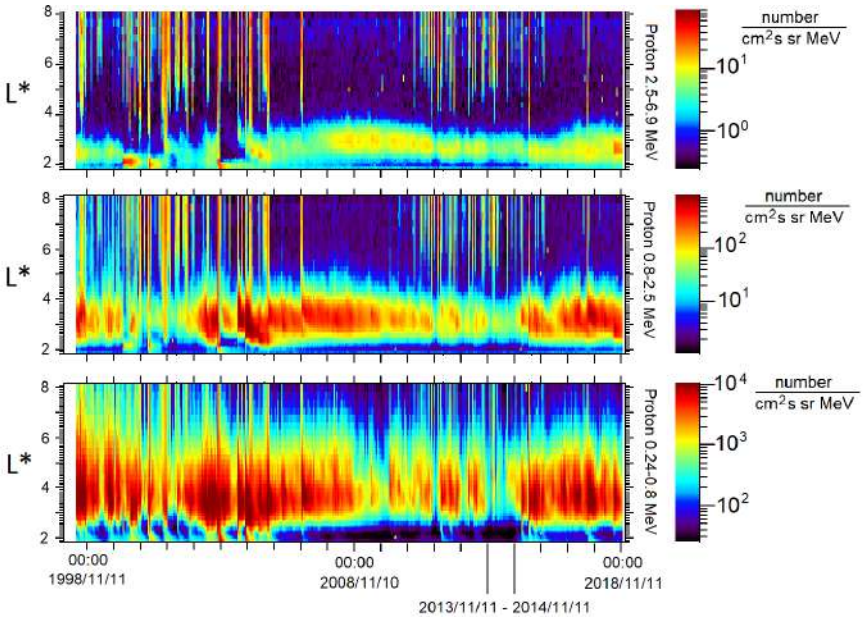

Figure 13: L-time cartographies of unidirectional proton flux measured by NPOES-15/SEM2 for several energies: 0.24-0.8 MeV (at the bottom), 0.8-2.5 MeV (in the middle) and 2.5-6.9 MeV (at the top), [20]. L^* is the radius (in Earth radii) of a particle's drift around the Earth if the magnetic field adiabatically relaxed to a dipole configuration. The graph shows flux drop in the bottom and middle panes around 2013/11/ – 2014/11/.

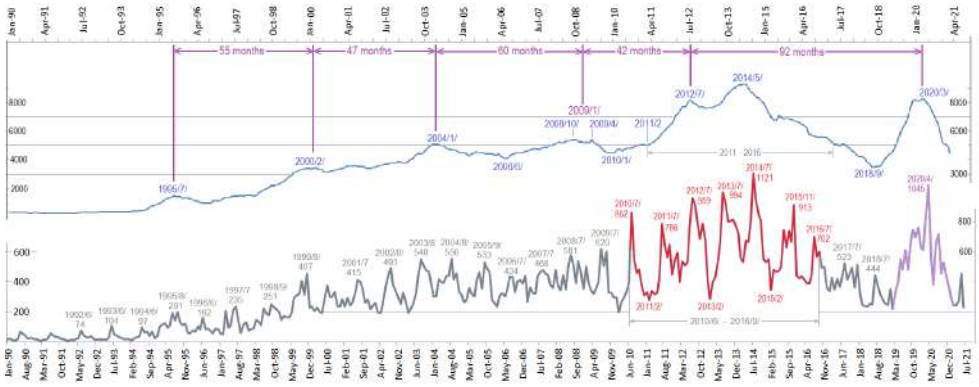

Figure 14: The bottom graph shows monthly global UFO sightings reported in 1990 – 2020, [26]. The top graph shows annual global sightings, the value for each month is calculated by adding the number of sightings in the month, in the preceding 6 months, and in the following 5 months. Pre-1995 counts are mostly in two digits and present too little information to be meaningful. Past-2018 data is likely to be corrupted by Starlink satellites.

explained. Thus it is not totally inconceivable that in mid-2014 – early-2015 sufficiently many energetic particles in the Van Allen Belts got accelerated to the energies of cosmic rays to produce the undulations. At other times, the Van Allen Belts may not produce enough high energy particles to affect the reading of cosmic ray monitors, but they certainly hurl enough energetic particles into the atmosphere to affect the atmosphere's temperature.

If energetic particles from the Van Allen Belts contributed to the undulations, we may expect the number of particles in the Van Allen Belts to drop around the time of the undulations. Indeed, Figure 12 shows that the high-energy electron flux drastically dropped around the time of the undulations, the mid-point of the drop falls on 2017/7/; Figure 13 shows that the proton flux also decreased around 2013/11/ – 2014/11/, the mid-point falls on 2014/6/. Although 27-day variability is easily seen in Figure 12, it is especially well-pronounced during 2014/8/ – 2015/5/ in the top four rows. Recently considered 2014/8/25 – 2014/10/4 subperiod of the undulations was shown to comprise three stages corresponding to intervals of increase/decrease in Figure 11: 1) 2014/8/27 – 2014/9/7, similar to HILDCAA; 2) 2014/9/13-20 with low flux of high energy electrons; and 3) 2014/9/22 – 2014/10/2, also similar to HILDCAA, [24].

3.4 UFO sightings as a measure of energy transfer from near-Earth environment to the Earth's atmosphere

Almost daily encounters of US Navy pilots with undetermined aerial objects high in the skies over the East Coast from the summer of 2014 to March 2015 reported by the US Defense Department, [25], suggest that the energetic particles entering Earth's atmosphere may produce lumps of highly-energetic secondary particles perceived by people as UFOs. Figure 14 shows monthly and annual UFO sightings, they were considerably above average in 2011 – 2016, reaching the all-time high at the time of the undulations in 2014/7/. As Figure 15 shows, the 1960 – 2010 portions of the graphs of UFO sightings and the speed of the magnetic North Pole are remarkably similar; the graphs differ in 2010 – 2016 due to the synchronization of Full Moon and perigee. Figure 17 shows a remarkable correlation between monthly UFO sightings and the bottom part of Figure 13 around 2010 – 2016.

Since energetic particles in the Earth's atmosphere are expected to increase the latter's tempera-

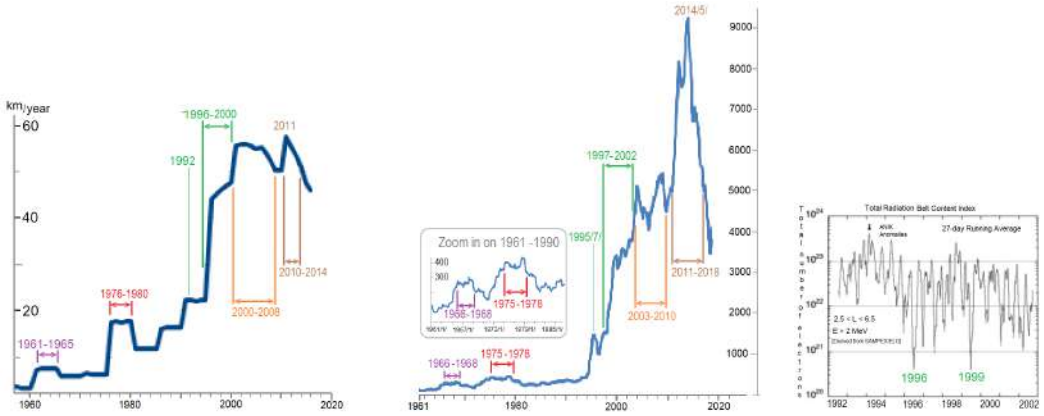

Figure 15: The graph on the left shows the speed of the magnetic North Pole based on the magnetic North Pole's location on January 1 of the year, [4]; the graph in the middle shows the annual global UFO sightings for 1961 – 2020, [26], the inset zooms in on the 1961 – 1990 period. The graphs are not identical but exhibit very similar overall behavior, similar features are emphasized with similarly-colored labels. The speed of the magnetic North Pole does not appear to have counterparts of the 2004/1/ and 2009/1/ UFO peaks; however, Figure 16 shows that the graph of the magnetic North Pole's speed does exhibit such counterparts if the resolution is even slightly improved. The graph on the right shows the total Radiation Belt Content index for the period 1992 – 2000 (monthly smoothing), [27]; two drastic drop-downs occurred in 1996 and 1999, right at the time of the two drastic increases in the magnetic North Pole's speed.

Data for inset **III**

Date	Coordinates of the magnetic North Pole	km moved in preceding 6 months	speed
1998/7/1	80.3N 108.067W		
1999/1/1	80.576N 108.597W	32	
1999/7/1	80.7N 109.13W	17	49
2000/1/1	80.972N 109.640W	32	49
2000/7/1	81.2N 110.30W	28	60
2001/1/1	81.427N 111.008W	28	56
2001/7/1	81.67N 111.78W	30	58
2002/1/1	81.879N 112.532W	26	56
2002/7/1	82.1N 113.35W	28	54
2003/1/1	82.325N 114.231W	28	56
2003/7/1	82.5N 114.96W	22	50
2004/1/1	82.762N 116.119W	33	55
2004/7/1	83.0N 117.24W	31	64
2005/1/1	83.186N 118.218W	24	55
2005/7/1	83.4N 119.38W	28	52
2006/1/1	83.602N 120.592W	27	55
2006/7/1	83.8N 121.88W	27	54
2007/1/1	83.995N 123.216W	27	54
2007/7/1	84.2N 124.78W	29	56
2008/1/1	84.363N 126.100W	23	52

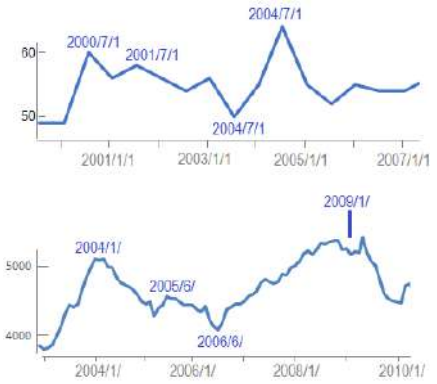

Figure 16: The table on the left shows the magnetic North Pole's coordinates on January 1 and estimated coordinates on July 1 of the year, the speed is the distance covered in the preceding 12 months. So-defined speed is a slight improvement in resolution on the definition used in Figure 15. The top graph shows the speed of the magnetic North Pole, while the bottom graph zooms in on the 1961 – 1990 period of the UFO graph in Figure 15. The 2004/1/ and 2009/1/ peaks in UFO sightings correspond to the 2000/7/1 and 2004/7/1 peaks in the speed of the magnetic North Pole.

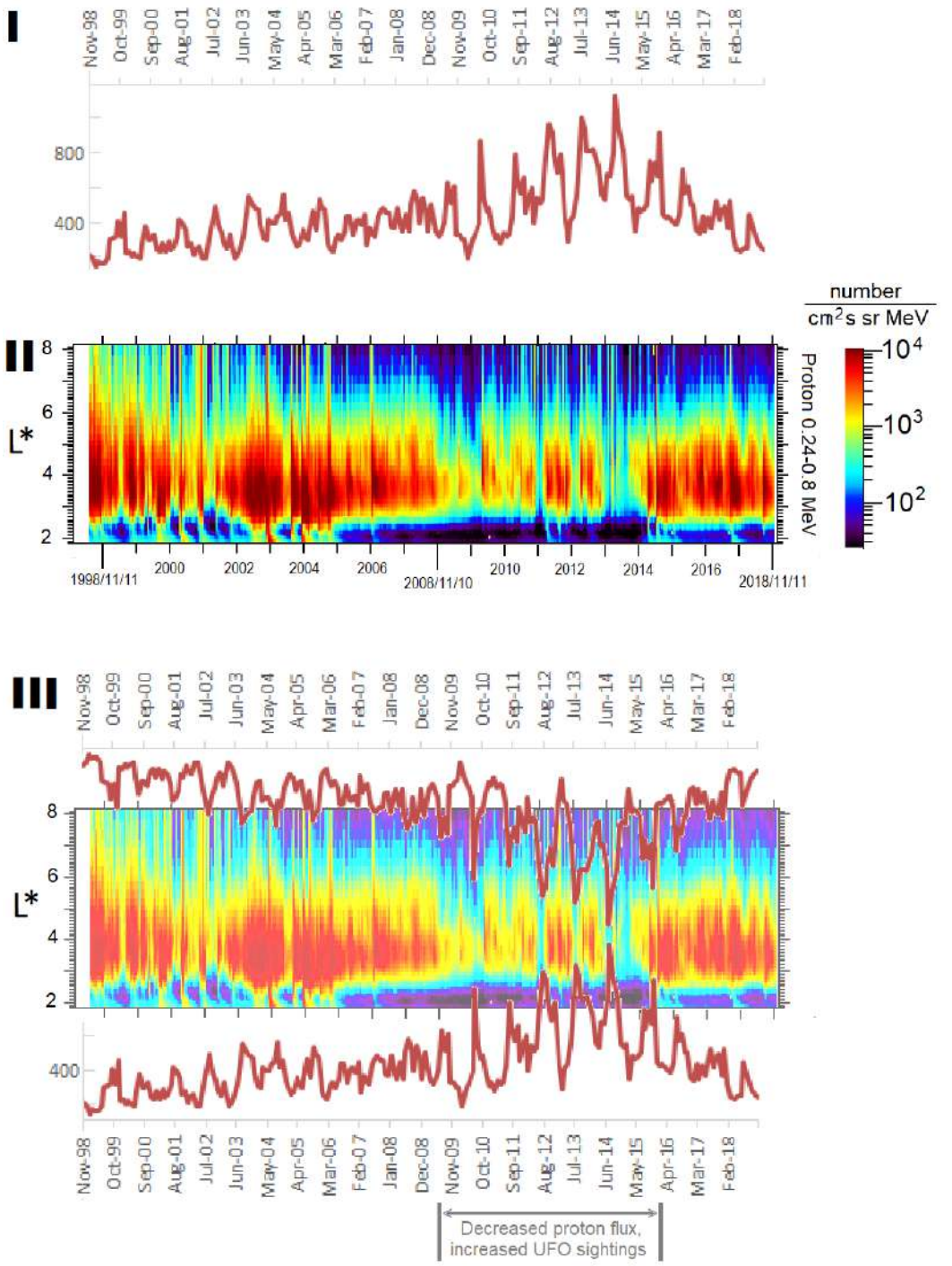

Figure 17: Frame I shows monthly UFO sightings from Figure 14, frame II shows the bottom part of Figure 13. In frame III, the graph from frame I and its inversion are superimposed on frame II with a ≈6.5-month lag. UFO sightings mirror proton flux: the maxima in UFO sightings more-or-less coincide with the gaps between maxima in proton flux; that is especially well-pronounced in 2010 – 2016. The highest number of UFO sightings corresponds to extremely low proton flux for L¡ 2.5.

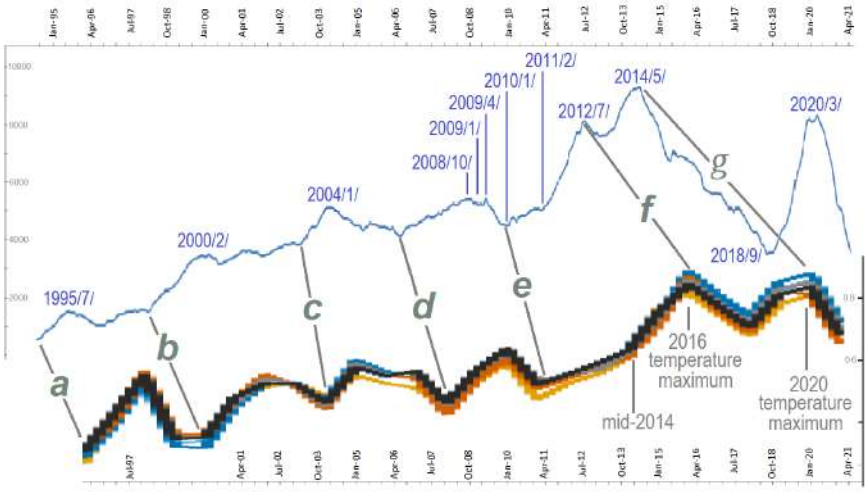

Figure 18: The top graph is the 1995/1/ – 1921/4/ annual global UFO sightings from Figure 14; the bottom graph is the 1996/3/ – 2019/12/ portion of Figure 1. The gray lines a - g divide both graphs into similar parts; the parts of the two graphs between each pair of consecutive gray lines are quite similar suggesting that the processes described by the two graphs are related. Lines *e* and *f* enclose both the largest uninterrupted temperature increase in the bottom graph and the largest uninterrupted increase in annual UFO sightings in the top graph. The 2014 and 2020 temperature maxima correspond to the 2012/7/ and 2014/5/ UFO maxima. The 2020 temperature maximum was only a few months after the first detection of Covid19.

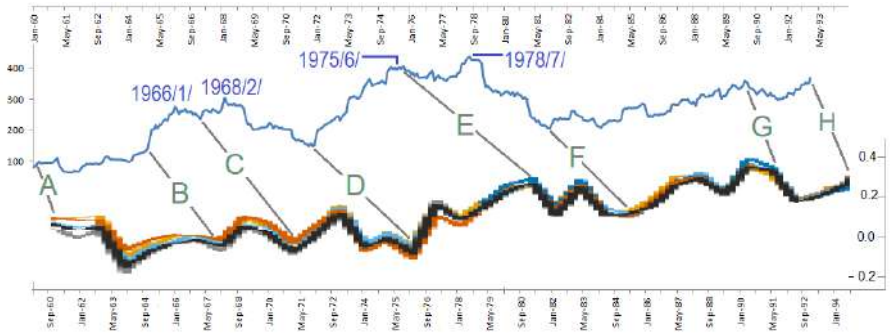

Figure 19: The top graph shows the annual global UFO sighting for 1960/1/ – 1993/1/ from Figure 14; the value for each month is calculated just like in Figure 18. The bottom graph is the 1960/9/ – 1994/9/ portion of Figure 1. Due to a rather small number of reported UFO sightings, the UFO graph does not properly reflect particle emissions from the Van Allen Belts, yet there is still some similarity between the graphs. The gray lines A - H divide both graphs into somewhat similar parts. The 1989/3/ – 1991/6/ period was marked by heavy bombardment with solar flares, of which twelve were $\geqslant X9.3$; in no other time has the Earth been known to be hit by so many powerful solar flares.

ture, we may expect a good correlation between the UFO sightings and temperature. Indeed, Figure 18 shows a remarkable similarity between the graph of the annual global UFO sightings in 1995/1/ – 1921/4/ and that of temperature anomalies in 1996/3/ – 2019/12/; the similarity of the two graphs suggests that such energetic particles affect Earth's temperature and are the main cause of current global warming. Even though pre-1995 UFO data contains too few sightings, Figure 19 reveals some similarity between the graphs of the annual global UFO sightings and temperature anomalies in 1960/1/1 – 1994/9/1; pre-1960 data is too sparse and spotty to be of any use. Unfortunately, the post-2018 UFO data is likely to be corrupted by Starlink satellites reported by some as UFOs; so it is hard to make any future forecasts based on UFO sightings. Figure 18 suggests that global temperature will go down for several years; what happens afterward depends on whether the 2020/3/ maximum in UFO sightings is a true maximum or a result of reports of Starlink satellites.

3.5 Other facets of global warming

Figure 20 shows NOAA's graphs of cold and warm temperature records for January - November. The graphs indicate that cold records prevailed from the first year of the graphs 1950 until 1990 – 1992, that is when the speed of the magnetic North Pole was $\leqslant 17$ km/year; while warm records have been prevailing since 1996 – 1997, when the speed of the magnetic North Pole was $\geqslant 20$ km/year. Since NOAA does not provide annual records, in Figure 21 all monthly records of Figure 20 are superimposed together, the obtained graph shows a remarkable correlation with the speed of the magnetic North Pole in 1951 – 2009.

The correlation of global temperature in 1900 – 2010 with the speed of the magnetic North Pole and the magnetic South Pole's rather sloth-like movement suggest that the largest temperature increase should be expected in the area around the two northern maxima of the total intensity of the Earth's magnetic field defined in Figure 9 and/or the magnetic North Pole, Figure 22 shows that it is indeed so, and the highest temperature increases are between the two northern maxima of the total intensity of the Earth's magnetic field; the very highest increase is right in front of the magnetic North Pole. While the parameters in Figure 22 were chosen by NASA to dramatize the effects of global warming, Figure 23 provides a somewhat more balanced view; it shows that the two northern maxima of the total intensity of the Earth's magnetic field built two patches of increased temperature near them by 2009, in 2009 – 2012 a nexus developed between the patches along the path of the magnetic North Pole, by 2016 the nexus had widened to create a single large spot that extended to Europe by 2021. Figures 22, 23 illustrate how inextricably linked are the increasing temperature and the Earth's magnetic field.

Figure 24 reveals that even powerful seismic activity in 1900 – 2015 seems to have followed the same pattern as global temperature and the speed of the magnetic North Pole.

With an increased number of aforementioned lumps of secondary energetic particles perceived as UFOs, one may expect an increased number of airplane accidents. Indeed, 2013/11/29 – 2015/10/31 saw an unusually large number of commercial airplane accidents, those widely discussed in media are shown in Table 2, 960 people died in merely 701 days of 2013/11/29 – 2015/10/31. There was also a large number of close calls reported by crews of commercial airplanes, [30]. Eerie circumstances of one of the accidents are illustrated in Figure 25. Those who find the connection of airplane accidents to energetic particles far-fetched, should be reminded that the 1996/7/17 explosion of TWA 800 was preceded by a streak of light of unknown origin. The 1996 – 2002 airplane crashes were contemporaneous with the 1996 – 2000 increase in the speed of the magnetic North Pole and 1996 – 2002 increase in the annual UFO sightings.

Figure 1 shows low temperature during 1907 – 1911, likely due to a diminished contribution of energetic particles from the Van Allen Belts. We may speculate that, for whatever reason, the energetic particles at the time did not enter the Earth's atmosphere in the usual way but instead as a large lump causing the Tunguska explosion. The proximity of the Tunguska explosion to the North-Eastern maximum of the total intensity of the Earth's magnetic field speaks in favor of the

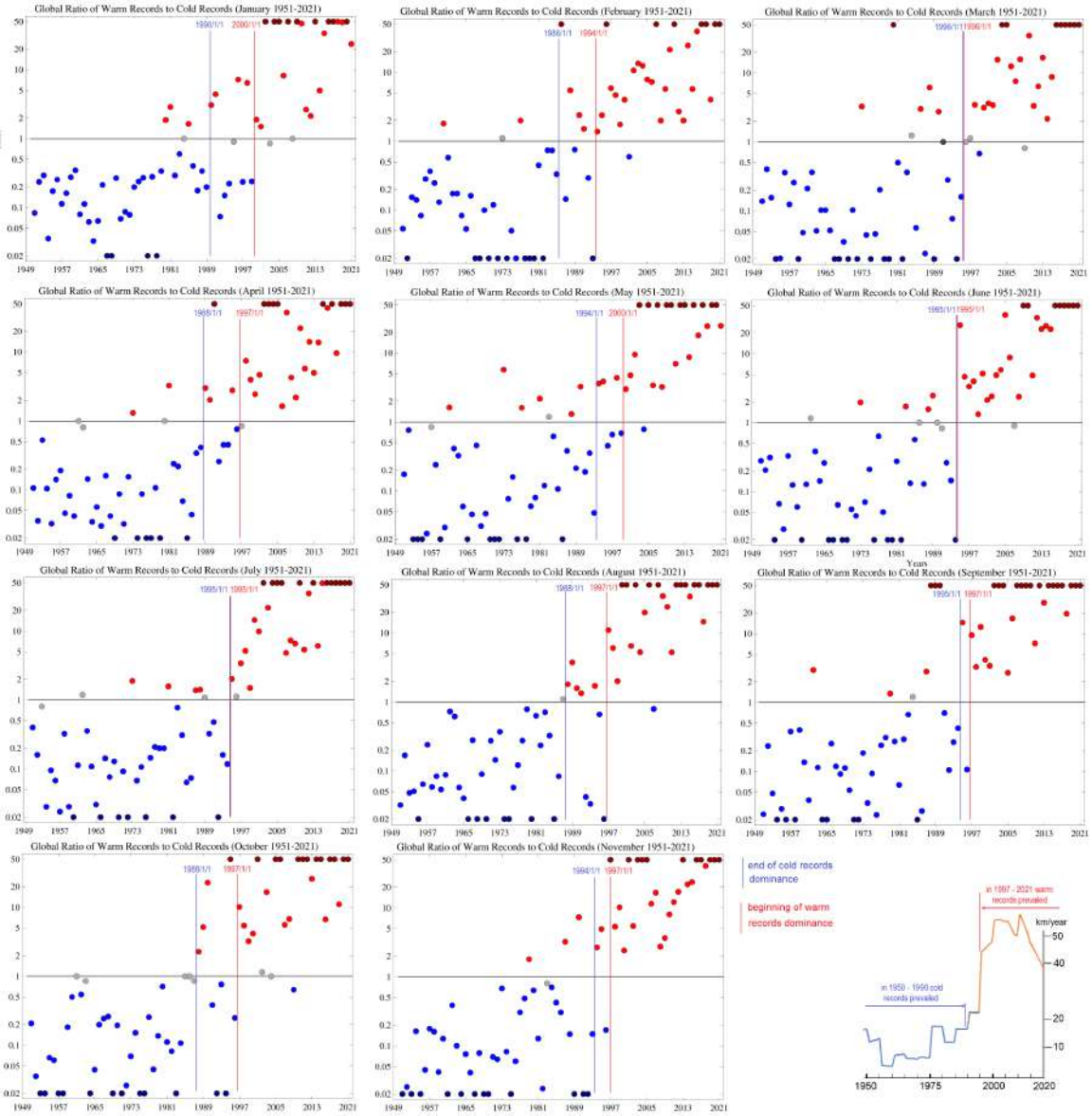

Figure 20: The ratio of warm-to-cold records for each month in 1951 – 2021, [28]; no data is available for December. A ratio value of X indicates that the global area experiencing record warm mean monthly temperatures over the most recent month was X times larger than the global area experiencing record cold conditions.

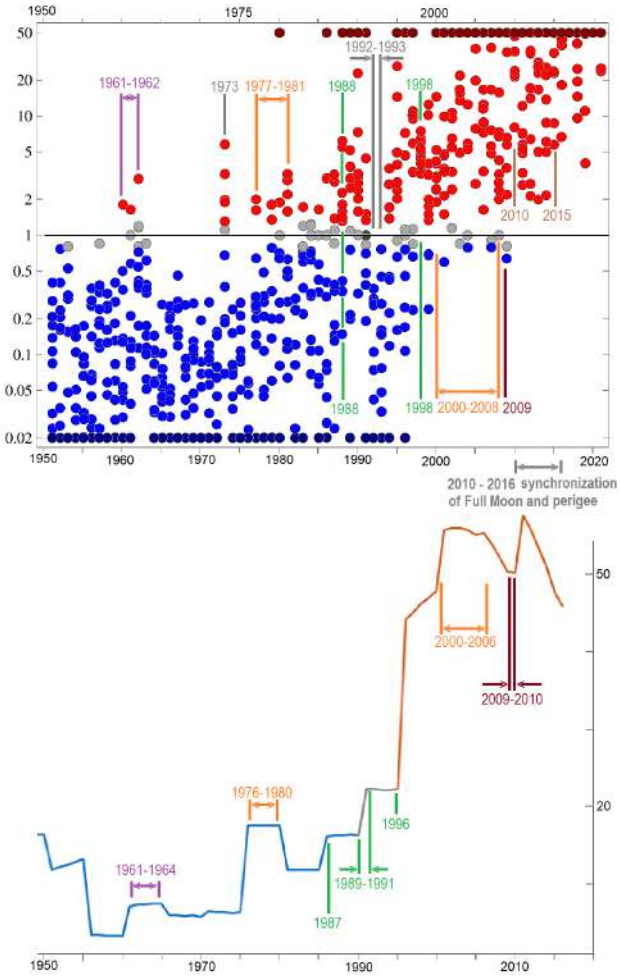

Figure 21: At the top, the 11 graphs of Figure 20 are superimposed together in one graph that shows a remarkable correlation with the speed of the magnetic North Pole at the bottom. The 1961 – 1964 slight increase in magnetic North Pole's speed almost coincided with the first $\geqslant 1$ ratios in 1960 – 1962; in 1976 – 1980 magnetic North Pole's speed rose to 17 km/year causing more significant $\geqslant 1$ ratios four years in a row in 1977 – 1981; the 1987 increase in the magnetic North Pole's speed to 16 km/year led to the first year of $\geqslant 1$ ratio prevalence in 1988; the VEI=6 eruption of Pinatubo and VEI=5 eruption of Hudson caused all ratios plunging to $\leqslant 1$ in 1992 – 1993; the 1996 drastic increase in the magnetic North Pole's speed to 44 km/year led to the prevalence of $\geqslant 1$ ratios in 1997 and no $\leqslant 1$ ratios in 1998; record high speed of the magnetic North Pole in 2000 – 2006 led to all ratios rising above 0.5 in 2000 and climbing above 0.2 in 2002 – 2008; the drop of the magnetic North Pole's speed to 50 km/year in 2009 resulted in the smallest ratio since 2001 in 2009; the beginning of the Full Moon and perigee synchronization in 2010 led to all ratios rising to $\geqslant 2$ in 2010 – 2021; the mid-2014 – early-2015 period led to all ratios rising to $\geqslant 4$ in 2010 – 2021. The 1973 single-year increase in $\geqslant 1$ ratio was most likely caused by an unusually large number of increases in tidal force: 1972/12/19-21 Full Moon, perigee, and lunar node; 1973/1/2-4 perihelion and eclipse; 1973/1/16-18 perigee and eclipse; 1973/5/4-6 lunar node, New Moon and perigee; 1973/6/1-2 New Moon-perigee and lunar node; 1973/6/16 eclipse; 1976/6/29-30 perigee and eclipse; 1973/7/17 eclipse; 1973/11/10-23 Full Moon, perigee, and lunar node; 1973/12/10 perigee and eclipse; 1973/12/24 eclipse.

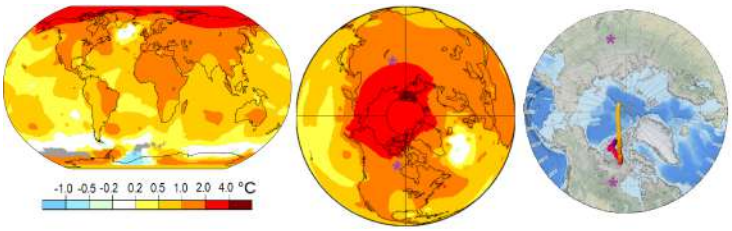

Figure 22: The left map shows NASA's average surface air temperatures increase in 2011 – 2021 compared to the 1956–1976 average; it indicates that the largest temperature increases have occurred in the Northern hemisphere. The map was generated with a smoothing radius of 1200 km. The middle map was generated using NASA's Scientific Visualization Studio generator with the same parameters as the top map, [31]. The modeled path of the magnetic North Pole in 1590 – 2022 is shown for reference only, [3]. The $\geqslant 2^{\circ}C$ temperature increase occurred around the two maxima of the total intensity of the Earth's magnetic field defined in Figure 9; the $\geqslant 4^{\circ}C$ temperature increase occurred close to the current magnetic North Pole's position. Purple asterisks mark approximate locations of the North-Eastern and North-Western maxima of the total intensity of the Earth's magnetic field in 2020.

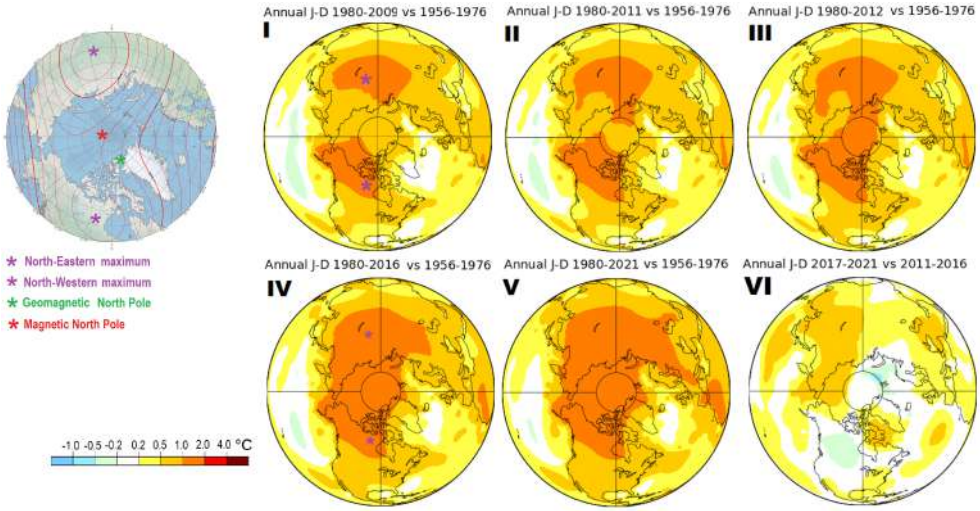

Figure 23: Evolution of the regions of $\geqslant 2^{\circ}C$ increase in the Northern hemisphere, generated using NASA's Scientific Visualization Studio generator using the same parameters as in Figure 22, [31]. On the left is a map of the total intensity of the Earth's magnetic field from WWM-2020 with the maxima of the total intensity of the Earth's magnetic field in 2020 marked by purple asterisks, provided as a reference only. Frame I shows two patches of increased temperature that formed near the two northern maxima of the total intensity of the Earth's magnetic field defined in Figure 9 by 2009; frames II and III shows the growth of a nexus connecting the two patches along the path of the magnetic North Pole in 2009 – 2012; frame IV shows how the nexus had widened by 2016 to create a single spot of increased temperature; frame V shows the moving of increased temperatures towards Europe. To avoid possible misinterpretation, frame VI is included to show that there was no drastic temperature increase in 2017 – 2021; the only left-over holdout of increasing temperature is around the North-Eastern maximum.

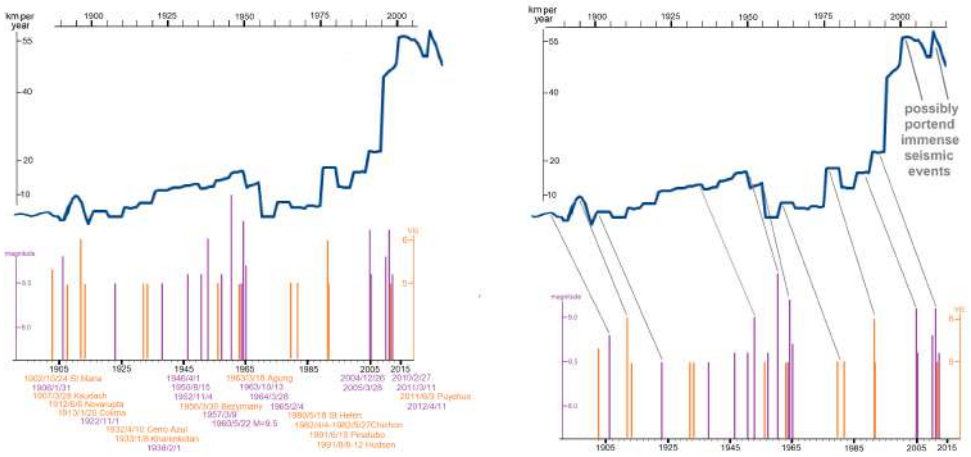

Figure 24: In the left pane, the speed of the magnetic North Pole is compared to the magnitude $\geqslant 8.5$ earthquakes, shown in purple, and VEI $\geqslant 6$ eruptions, shown in orange, in 1900 – 2015, [10, 14]. VEI=6 eruptions and magnitude $\geqslant 9.0$ earthquakes are represented by lines of the same height as the frequencies of VEI=6 eruptions and magnitude $\geqslant 9.0$ earthquakes are about the same; there were five VEI $\geqslant 5$ eruptions and four magnitude $\geqslant 9.0$ earthquakes in 1900 – 2021. The right frame shows the same graphs but with the time scales synchronized, gray lines connect powerful seismic events with the corresponding increases in the speed of the magnetic North Pole. The two graphs move in tandem in $\approx 1900 - 1996$, with seismic activity; each surge in the speed of the magnetic North Pole corresponds to a cluster of 1 - 3 seismic events $\approx$15 years later. The post-1996 high values of the magnetic North Pole's speed have no corresponding seismic events as if portending upcoming seismic events of immense proportions.

hypothesis. A partial hint at the origins of the Tunguska explosion might be furnished by a meteor detected on 2014/1/8, its unusually high heliocentric velocity at impact is presented as a proof of its out-of-the-Solar-System origin, [34]. Yet, it is hard to believe that this one-of-a-kind guest arrived on Earth merely by chance just a few months before the mid-2014 – early-2015 undulations and within a week of the 2014/1/1 New Moon-perigee, 2014/1/4 perihelion, 2014/1/5 Jupiter opposition, 2014/1/1/11 Venus conjunction, that is when the tidal force was close to an all-time high. Much more likely is that the meteor was just a highly energetic UFO created by energetic particles from the Van Allen Belts.

4 Conclusions

The current global warming has been attributed to increased levels of CO_2; yet, the graphs of temperature and CO_2 bear no resemblance. In 1900 – 2010 global temperature practically mirrored the behavior of the magnetic North Pole's speed, following a similar but somewhat more complicated pattern in the preceding centuries. The drastic increase in global temperature, the speed of the magnetic North Pole, and UFO sightings started shortly after the 1989 – 1991 heavy bombardment by powerful solar flares. The areas most affected by global warming were near the two northern maxima of the total intensity of the Earth's magnetic field and the magnetic North Pole. In 2010 – 2016, the influence of the Earth's magnetic field on the global temperature and UFO sightings was augmented by the increase in tidal force due to the 2010 – 2016 synchronization of Full Moon

Date & deaths		Airline, flight number, and a comment
		NO SUCH ACCIDENTS IN 2017– 2021
2016/5/19	66	EgyptAir 804, undetermined cause with evidence of fire onboard
2015/10/31	224	Metrojet 9268, undetermined cause, but blamed on terrorists
2015/3/24	150	Germanwings 9525, attributed to the co-pilot's suicide
2014/12/27	162	AirAsia 8501, captain removed breaker to cut power
2014/7/24	116	Air Algerie 5017, obstruction of pressure sensors
2014/7/23	48	TransAsia Airways 222, unusual sounds before the crash, blamed on the crew
2014/3/7	227	Malaysia Airlines 370, just vanished
2013/11/29	33	LAM Mozambique Airline 470, attributed to the pilot's suicide
2009/6/1	228	Air France 447, attributed to the crew's mistakes
2005/10/25	117	Bellview Airlines 210, undetermined cause
2002/5/25	225	China Airlines 611, attributed to fatigue cracking
1999/10/31	217	EgyptAir 990, attributed to the pilot's suicide
1998/9/2	229	Swissair 111, onboard fire of unknown origin
1997/12/19	104	SilkAir 185, attributed to the captain's suicide
1996/7/17	230	TWA 800, an explosion of a fuel tank following a hit by a streak or flash of light of unknown origin
1994/8/21	44	Royal Air Maroc 630, attributed to pilot's suicide
		NO SUCH ACCIDENTS IN 1990 – 1993

Table 2: Unexplained, or incompletely explained commercial/civilian airplane accidents in 1990 – 2021 with ¿30 fatalities much discussed in mass media, [32]. The six crashes in the 16 months of 2013/11/29 – 2015/3/24 averaged a crash every 3 months. Never before or after so many commercial airplanes crashed in such a short time. There were two accidents within 24 hours in July 2014, the unusual circumstances of one of them are discussed in Figure 25. Each accident may be googled for more information. Dates are linked to Aviation Safety Network, airlines with flight numbers are linked to Wikipedia articles. This table includes all but one airplane crashes with $\geqslant 8$ fatalities attributed to a pilot's suicide; 1982/2/9 Japan Air Lines 350 is excluded as the survivors confirmed it was indeed an attempted suicide. The fires inside aircraft could be caused by fireballs, appearance of fireballs inside aircraft was discussed in Paul Sagan's book "Ball lightning: paradox of Physics", section Dangerous Aircraft Encounters.

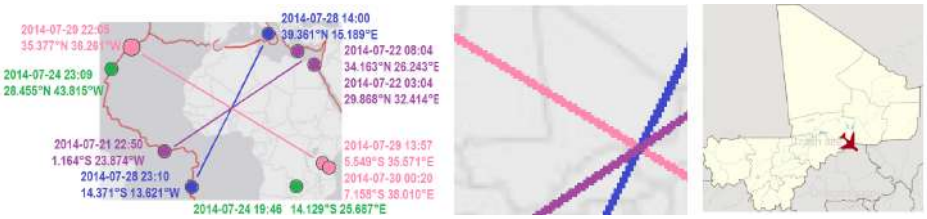

Figure 25: The right pane shows the crash site of Air Algeirie 5017 on 2014/7/24, [33]. The left pane shows magnitude$\geqslant$ 4 earthquakes from 2014/7/21 22:00 UTC to 2014/7/30 1:00 UTC in$15^\circ S - 40^\circ N, 44^\circ W - 39^\circ E$, [10]. Quakes marked by the same color struck within 9.25 hours of each other, which we may consider being almost simultaneous. The line connecting one quake marked purple with the point between the other two, the line connecting the quakes marked pink, and the line connecting the quakes marked blue intersect at the same point, which is very close to the crash site of Air Algeirie 5017. The straight lines, of course, represent great circles on the globe. The three lines look like a giant reticle pointing at the Air Algeirie 5017 crash site. The middle pane zooms in on the intersection point to demonstrate how close it is to the crash site. This is an example of a rare phenomenon of the *seismic cross hairs*, its anatomy is to be discussed elsewhere.

and perigee. The demonstrated correlation between global temperature, movement of the magnetic North Pole, and UFO sightings cannot be explained by increased levels of CO_2 but can be explained by our hypothesis.

Truly bewildering is the currently popular view that different geophysical phenomena such as earthquakes and eruptions, movement of the magnetic poles, auroras, etc. are unrelated to each other; hardly can be attributed to a mere coincidence the concomitance of 1) an unusually high frequency of unexplained or incompletely-explained airplane accidents in 2013/11/29 – 2015/10/31 illustrated by Table 2; 2) almost daily encounters of US Navy pilots with undetermined aerial objects from the summer of 2014 to March 2015, [25]; 3) the all-time high of UFO sightings in the middle of 2014 in Figure 14; 4) unusual and never-before-seen undulations of Figure 11; 5) the only known case of a space hurricane detected on 2014/8/20, [16]; 6) depletion of the Van Allen Belts around 2014 illustrated by Figures 12, 13; 7) a sudden jump in the derivative of global temperature in mid-2014 exhibited in Figure 1. Already in 1923 in his book *New Lands*, Charles Fort suggested that so-called UFOs were coming from near-terrestrial space; while in the 1950s, Dr J. Allen Hynek suggested that the so-called UFOs are likely to be a natural phenomenon. It is quite likely that some, if not all, airplane accidents of Table 2 were caused by lumps of highly-energetic secondary particles perceived by people as UFOs; had proper research been done, the disasters might have been mitigated.

Acknowledgement

The author would like to thank all people who produced and provided material used in this article. He would also like to thank all who took time and effort to patiently explain the aspects of the paper the author was not familiar with.

Competing Interests

The author declares that no competing interests exist."

References

[1] Global temperature, https://public.wmo.int/en/media/press-release/state-of-climate-2021-extreme-events-and-major-impacts, https://climate.metoffice.cloud/temperature.html. An interactive graph is available at https://ourworldindata.org/co2-and-other-greenhouse-gas-emissions.

[2] The graphs of pre-1900 solar activity determined from proxies are from https://en.wikipedia.org/wiki/File:Carbon14_with_activity_labels.svg, https://wattsupwiththat.com/2008/12/29/don-easterbrooks-agu-paper-on-potential-global-cooling/, Usoskin, I.G., S.K. Solanki, N.A. Krivova, B. Hofer, G A. Kovaltsov, L. Wacker, N. Brehm and B. Kromer, Solar cyclic activity over the last millennium reconstructed from annual 14C data, Astron. Astrophys., 649, A141 (2021), https://arxiv.org/pdf/2103.15112.pdf.

[3] NOAA, Modelled magnetic poles' paths, https://www.ncei.noaa.gov/maps/historical_declination/. Proper boxes need to be checked.

[4] Williams, B., The Correlation of North Magnetic Dip Pole Motion and Seismic Activity, *Journal of Geology and Geophysics*, 2016, https://www.longdom.org/open-access/the-correlation-of-north-magnetic-dip-pole-motion-and-seismic-activity-2381-8719-1000262.

pdf, data from https://www.ngdc.noaa.gov/geomag/data/poles/NP.xy. The graph was kindly emailed to the author of the paper on 2021/1/1.

[5] Mean Central England Temperature, https://www.metoffice.gov.uk/hadobs/hadcet/, https://www.metoffice.gov.uk/hadobs/hadcet/cet_info_mean.html, based on Parker et al (1992), https://www.metoffice.gov.uk/hadobs/hadcet/Parker_etalIJOC1992_dailyCET.pdf. Numerical dataset https://www.metoffice.gov.uk/hadobs/hadcet/cetml1659on.dat.

[6] Schroeder, W., On the Existence of the 11-Year Cycle in Solar and Auroral Activity before and during the so-called Maunder Minimum, *Journal of geomagnetism and geoelectricity*, 1992 vol. 44 issue 2 pp.119-128, https://www.jstage.jst.go.jp/article/jgg1949/44/2/44_2_119/_article.

[7] Hiebl, J., The early instrumental climate period (1760–1860) in Europe, evidences from the Alpine region and Southern Scandinavia, thesis, https://www.meteologos.rs/wp-content/uploads/2019/12/THE-EARLY-INSTRUMENTAL-CLIMATE-PERIOD-IN-EUROPE_1760-1860.pdf

[8] NOAA's maps https://www.ngdc.noaa.gov/geomag/magfield-wist/, database https://www.ngdc.noaa.gov/geomag/calculators/magcalc.shtml#igrfgrid.

[9] NASA's Solar System calculator, https://www.fourmilab.ch/cgi-bin/Solar.

[10] USGS earthquake catalog https://earthquake.usgs.gov/earthquakes/search/ and NOAA earthquake database https://www.ngdc.noaa.gov/hazel/view/hazards/earthquake/search.

[11] Space Weather Archives, http://www.solarstorms.org/SRefStorms.html.

[12] Lunar data http://astropixels.com/ephemeris/moon/moonnodes2001.html and https://www.fourmilab.ch/earthview/pacalc.html

[13] Jupiter syzygies. For 2002 – 2021 http://iaaras.ru/media/data/ae2021/ae_d4e.txt with the year appropriately selected; for 1991 – 2021 https://www.planetary.org/articles/06031044-oppositions-conjunctions-rpx; for 1990 – 2021 *Astronomical Phenomena for the Year 2021* with 2021 replaced by the required year; for 1912 – 1989 *Observer's handbook 1989* at https://www.rasc.ca/sites/default/files/publications/ObserversHandbook-1989.pdf with 1989 replaced by the required year from. Non-scientific http://www.astrology.com.pl/transits/2021/ with 2021 replaced by the appropriate year might be the most convenient to use.

[14] Eruptions databases, https://www.ngdc.noaa.gov/hazel/view/hazards/volcano/event-search, https://volcano.si.edu/search_eruption.cfm.

[15] Van Allen Belts in 2012, https://www.science.org/doi/10.1126/science.1233518, https://www.scientificamerican.com/article/third-van-allen-radiation-belt-makes-appearance-around-earth/

[16] Qing-He Zhang et al, A space hurricane over the Earth's polar ionosphere, *Nature Communications*, vol. 12, article number: 1207 (2021), https://www.nature.com/articles/s41467-021-21459-y.

[17] Moscow Neutron Monitor http://cr0.izmiran.ru/mosc/main.htm, Oulu Neutron Monitor https://cosmicrays.oulu.fi/. Other monitors and data https://www.nmdb.eu/nest/, http://neutronm.bartol.udel.edu/.

[18] Yulbarisov, R., Galikyan, N., Mayorov, A. et al. Amplitude and Temporal Characteristics of 27-Day Variations in the Galactic Cosmic Ray Flux, Measured during the PAMELA Experiment between 2006 and 2016. Bull. Russ. Acad. Sci. Phys. 85, 1272–1275 (2021). https://doi.org/10.3103/S1062873821110381.

[19] Turner, D., O'Brien, T., Fennell, J., Claudepierre, S., Blake, J., Jaynes, A., Baker, D., Kanekal, S., Gkioulidou, M., Henderson, M., Reeves, G., Investigating the source of near-relativistic and relativistic electrons in Earth's inner radiation belt, *GJR Space Physics,* vol. 122, issue1, 2017, pp. 695-710, https://agupubs.onlinelibrary.wiley.com/doi/full/10.1002/2016JA023600. Similar graphs at https://angeo.copernicus.org/preprints/angeo-2018-98/angeo-2018-98.pdf.

[20] Sicard, A., Bourdarie, S., Lazaro, D., Standarovski, D., Ecoffet, R., et al. A new model for the 1-10 MeV proton fluxes (part of ONERA GREEN-V3 model). European Conference on Radiation and its Effects on Components and Systems (RADECS) 2019, Montpellier, France. https://hal.archives-ouvertes.fr/hal-02797017/document

[21] Allison, H., Shprits, Yu., Local heating of radiation belt electrons to ultra-relativistic energies, *Nature Communications,* 2020; 11: 4533, https://www.ncbi.nlm.nih.gov/pmc/articles/PMC7483540/.

[22] Allison, H., Shprits, Yu., Zhelavskaya, I., Wang, D., Smirnov, A., Gyroresonant wave-particle interactions with chorus waves during extreme depletions of plasma density in the Van Allen radiation belts, *Science Advances*, 2021, Vol 7, Issue 5, https://www.science.org/doi/10.1126/sciadv.abc0380.

[23] Zhang, X., Artemyev, A., Angelopoulos, V. et al. Superfast precipitation of energetic electrons in the radiation belts of the Earth. Nat Commun 13, 1611 (2022). https://www.nature.com/articles/s41467-022-29291-8#citeas

[24] Jaynes, A. N., et al. (2015), Source and seed populations for relativistic electrons: Their roles in radiation belt changes, J. Geophys. Res. Space Physics, 120, pp. 7240– 7254, https://agupubs.onlinelibrary.wiley.com/doi/10.1002/2015JA021234. The portion quoted is under Figure 4.

[25] *New York Times* https://www.nytimes.com/2019/05/26/us/politics/ufo-sightings-navy-pilots.html

[26] UFO Reporting Center, http://www.nuforc.org/webreports/ndxevent.html.

[27] Baker, D.N., Erickson, P.J., Fennell, J.F. et al. Space Weather Effects in the Earth's Radiation Belts. Space Sci Rev 214, 17 (2018), Figure 29. https://link.springer.com/article/10.1007/s11214-017-0452-7

[28] NOAA, Global area at record levels for 1951 – 2021. To access a specific month use link https://www.ncdc.noaa.gov/sotc/global/2021XX/supplemental/page-3 with XX replaced by 01 for January, 02 for February, ..., 11 for November; there is no data for December. For example, July may be accessed at https://www.ncdc.noaa.gov/sotc/global/202107/supplemental/page-3, it is also available at https://commons.wikimedia.org/wiki/File:202107_Percent_of_global_area_at_temperature_records_-_Global_warming_-_NOAA.svg.

[29] Most powerful solar flares known, https://www.spaceweatherlive.com/en/solar-activity/top-50-solar-flares.html, http://www.ioffe.ru/LEA/Solar/1994_en.html, https://www.spaceweather.com/solarflares/topflares.html, https://www.sws.bom.gov.au/Educational/2/3/9.

[30] Nine confirmed close-call encounters with UFOs: a) 2016/11/14 https://www.thestar.com/news/canada/2016/11/14/porter-plane-in-near-miss-with-drone.html; b) 2016/4/17 https://www.theguardian.com/technology/2016/apr/28/heathrow-ba-plane-strike-not-a-drone-incident, c) 2015/4/7 http://www.denverpost.com/business/ci_27872975/denver-bound-icelandair-flight-from-reykjavik-hit-by; d) 2014/12/15 https://en.wikipedia.org/wiki/Loganair_Flight_6780; e) 2014/11/5 http://avherald.com/h?article=47d74074; f) 2014/3/19 http://

www.atsb.gov.au/media/4897226/AO-2014-052%20Final.pdf; g) 2013/7/19 http://www.huffingtonpost.com/2014/01/06/ufo-jet-airliner-near-miss-over-uk_n_4549399.html; h) 2013/6/4 http://www.dailymail.co.uk/news/article-2339139/Was-bird-A-Plane-Or-UFO--Chinese-passenger-jet-hits-mysterious-object-26-000ft-lands-severely-dente html, http://cayodagyo.blogspot.com/2013/06/some-possibilities-of-object-that-had.html; i) 2012/12/2 http://www.ibtimes.co.uk/ufo-plane-glasgow-scotland-463308#.

[31] NASA's Scientific Visualization Studio generator is at https://data.giss.nasa.gov/gistemp/maps/index_v4.html; the parameters are taken from https://en.wikipedia.org/wiki/Instrumental_temperature_record, https://commons.wikimedia.org/wiki/File:Change_in_Average_Temperature.svg.

[32] Unexplained, or not completely explained civilian airplane accidents in 2013 – 2016 much discussed in mass media. Aviation Safety Network https://aviation-safety.net/ and Wikipedia. Crashes at takeoff or landing, crashes of Boeing 747 Max, crashes of military planes like https://en.wikipedia.org/wiki/2016_Indian_Air_Force_An-32_disappearance, and crashes of small aircraft like https://www.cbc.ca/news/canada/calgary/tsb-report-jim-prentice-plane-crash-release-1.4635541 are not included in the table.

[33] Air Algeirie 5017, https://en.wikipedia.org/wiki/Air_Alg%C3%A9rie_Flight_5017

[34] Siraj, A., Loeb, A., Discovery of a Meteor of Interstellar Origin, https://arxiv.org/pdf/1904.07224.pdf